Highlights

Numerical analysis of the twin tunnels with transverse galleries using plastic and viscous constitutive models for rockmass and lining

Quevedo, F. P. M.,Colombo, C. A. M. M.,Bernaud, D.,Maghous, S.

- Qualquer coisa 1
- Qualquer coisa 2
- Qualquer coisa 3

Numerical analysis of the twin tunnels with transverse galleries using plastic and viscous constitutive models for rockmass and lining

Quevedo, F. P. M.[a,*], Colombo, C. A. M. M.[a], Bernaud, D.[a] and Maghous, S.[a]

[a] *Federal University of Rio Grande do Sul, Av. Osvaldo Aranha, 99, Porto Alegre, 90.035-190, RS, Brazil*

ARTICLE INFO

Keywords:
twin tunnels
transverse gallery
constitutive models
finite element method

ABSTRACT

This paper aims to demonstrate the long-term implications of the rheological constitutive behavior of rock mass and concrete lining in the convergence of the intersection area of twin tunnel galleries using a three-dimensional numerical analysis based on the finite-element method. A Drucker-Prager-Perzyna elastoplastic-viscoplastic constitutive law represents the rock mass and, for the lining, an elastic and viscoelastic law. The deactivation-activation methods simulate the excavation process. Comparisons of convergence reveal that the viscous effects of the rock mass and the lining significantly influence the peak convergence within the intersection zone, resulting in differences of approximately 10% in convergence values.

1. Introduction

The structural design of deep twin tunnels involves estimating cross-section convergence, lining pressure, and the size of the plastic zone within the rock mass caused by the excavation process. The final convergence and stress field around the tunnel depend on *in situ* initial stresses, cross-section geometry, and the coupling between the lining and the rock mass during construction. Unlinke a single tunnel, the proximity between twin tunnels break the symmetry of deformations in tunnel wall. Many twin tunnels have transverse galleries that serve as emergency routes. These galleries will introduce a local effect on the convergence profile of the longitudinal tunnel.

Additionaly, the rheological behavior of the rockmass and lining plays a crucial role in how stress and displacements fields evolve over time.

Indicar os objectivos do trabalho e fornecer um contexto adequado, evitando uma pesquisa bibliográfica ou um resumo dos resultados.

2. Statement of problem and fundamental assumptions

3. Constitutive Model of the Rock Material

An elastoplastic-viscoplastic constitutive model was implemented in ANSYS using the UPF/USERMAT customization tool [1] to simulate rock mass. This model concern a serial association of the plastic and viscoplastic constitutive models, i.e., the total strain $\dot{\boldsymbol{\varepsilon}} = \dot{\boldsymbol{\varepsilon}}^e + \dot{\boldsymbol{\varepsilon}}^p + \dot{\boldsymbol{\varepsilon}}^{vp}$, which leads to the following linear constitutive relationship:

$$\dot{\boldsymbol{\sigma}} = \boldsymbol{D} : \dot{\boldsymbol{\varepsilon}}^e = \boldsymbol{D} : (\dot{\boldsymbol{\varepsilon}} - \dot{\boldsymbol{\varepsilon}}^p - \dot{\boldsymbol{\varepsilon}}^{vp}), \tag{1}$$

where $\dot{\boldsymbol{\varepsilon}}^e$, $\dot{\boldsymbol{\varepsilon}}^p$ and $\dot{\boldsymbol{\varepsilon}}^{vp}$, represent the elastic, plastic and viscoplastic strain rate, respectively. The one-dimensional representation in Fig. 1 shows this association.

*Corresponding author.

motta.quevedo@ufrgs.br (Q.F.P. M.); carlos.colombo@ufrgs.br (C.C.A.M. M.); denise.bernaud@ufrgs.br (B. D.); samir.maghous@ufrgs.br (M. S.)

https://www.researchgate.net/profile/Felipe-Pinto-Da-Motta-Quevedo (Q.F.P. M.); http://lattes.cnpq.br/4919388217690564 (C.C.A.M. M.); http://lattes.cnpq.br/2809615143819128 (B. D.); http://lattes.cnpq.br/6305244914209829 (M. S.)

ORCID(s): 0000-0003-4171-1696 (Q.F.P. M.); 0000-0000-0000-0000 (C.C.A.M. M.); 0000-0001-6365-3269 (B. D.); 0000-0002-1123-3411 (M. S.)

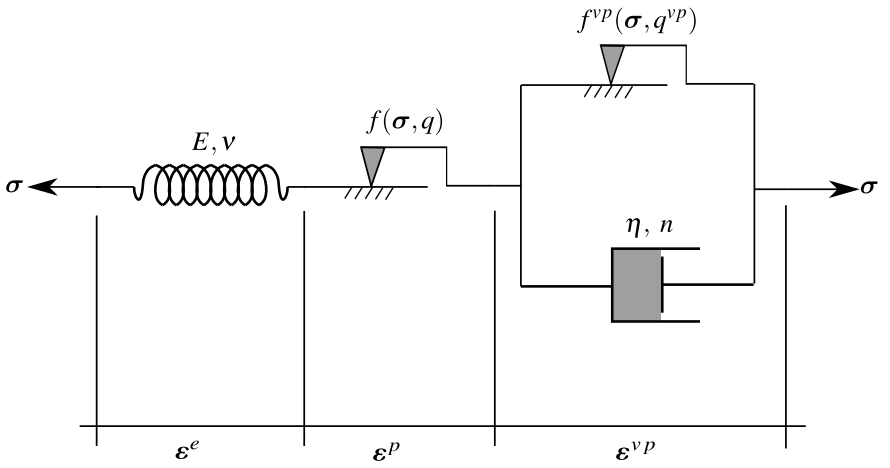

Figure 1: Rheological representation of the elastoplastic-viscoplastic model.

In this model is used a Drucker-Prager plastic flow surface given by

$$f(\boldsymbol{\sigma}, q) = f(I_1, J_2, q) = \beta_1 I_1 + \beta_2 \sqrt{J_2} - q(\alpha), \tag{2}$$

which I_1 is the first invariant of the stress tensor, J_2 the second invariant of the deviator tensor and β_1, β_2 and $q(\alpha)$ are strength parameters related to the friction angle ϕ and cohesion $c(\alpha)$, respectively. In the present model Drucker-Prager surface been inner of the Mohr-Coulomb surface [4], that is,

$$\beta_1 = \frac{(k-1)}{3}, \quad \beta_2 = \frac{(2k+1)}{\sqrt{3}}, \quad q(\alpha) = 2\sqrt{k}\, c(\alpha), \tag{3}$$

where $k = (1 + \sin\phi)/(1 - \sin\phi)$. The internal variable α is the equivalent plastic strain $\bar{\varepsilon}^p$ used to simulate strain hardening/softening phenomena. However, for this study, we adopt perfect plasticity, meaning that c is a constant. For the viscoplasticity surface f^{vp} the same surface is empolyed, but with ϕ^{vp} in β_1 and β_2, and $q^{vp} = 2\sqrt{k^{vp}} - c^{vp}$ where $k^{vp} = (1 + \sin\phi^{vp})/(1 - \sin\phi^{vp})$ and c^{vp} is a constant, i.e., perfect viscoplasticity.

The plastic flow rule is given by:

$$\dot{\boldsymbol{\varepsilon}}^p = \begin{cases} \dot{\lambda}\dfrac{\partial g}{\partial \boldsymbol{\sigma}} & \text{for } f > 0 \\ \mathbf{0}, & \text{for } f < 0 \end{cases}, \tag{4}$$

where $\dot{\lambda}$ is the plasticity multiplier and g is a potencial flow analogous to f to simulate the volume dilatation during the evolution of plastic deformations. However, for this analysis, was used associated plasticity, i.e., $g = f$. The plastic multiplier is obtained through the consistency condition $\dot{f} = 0$. Numerical details of this implementation can be found in [9]. For viscoplastic flow rule we have,

$$\dot{\boldsymbol{\varepsilon}}^{vp} = \dot{\lambda}^{vp}\frac{\partial f^{vp}}{\partial \boldsymbol{\sigma}} \tag{5}$$

In contrast to the plastic multiplier, the viscoplastic multiplier is independent of a consistency condition. As a result, its expression is explicit. For this study, we utilize the Perzyna model as follows:

$$\dot{\lambda}^{vp} = \frac{\Phi(\boldsymbol{\sigma}, q^{vp})}{\eta} \quad \text{and} \quad \Phi = \left\langle \frac{f^{vp}(\boldsymbol{\sigma}, q^{vp})}{f_0} \right\rangle^n, \tag{6}$$

where Φ is the overstress function, η is the dynamic viscosity constant, n is the dimensionless parameter that gives the form of the power law, f_0 a parameter conveniently adopted and $\langle * \rangle$ is the McCauley function which is 0 when $* < 0$, i.e. viscoplastic flow will only occur when the overstress function is positive.

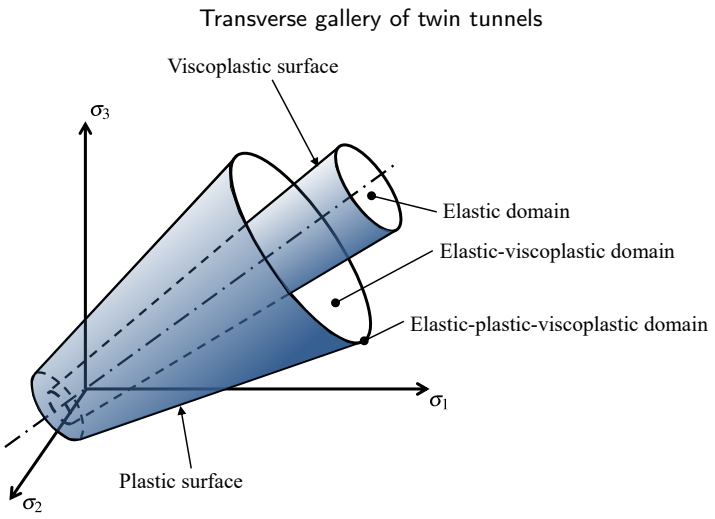

Figure 2: Elastoplastic-viscoplastic domains.

In this coupled model, when $\phi = \phi^{vp}$, cohesion entirely controls the evolution of local mechanical fields. Specifically, when $c \to \infty$ and $c^{vp} \to \infty$, the system achieves a purely elastic solution. The solution becomes purely elastoviscoplastic with $c \to \infty$, while a pure elastoplastic solution emerges with $c^{vp} \to \infty$. In this study's coupled analysis, we have adopted $c^{vp} < c$, allowing the viscoplastic domain to occur independently of plasticity. However, in the presence of plasticity, viscous effects become inevitable. Fig. 2 illustrates these domains in principal stress space.

Details of this model, including validations and its application in single tunnel, are in [9]. See [7] for the algorithm details implemented in FORTRAN within the USERMAT subroutine.

4. Constitutive Model of the Lining

We implemented a viscoelastic model in ANSYS using the UPF/USERMAT customization feature [1]. The model simulates concrete creep through a Generalized Kelvin chain, based on Bažant and Prasannan's Solidification Theory [2; 3], with parameter adjustments performed using the CEB-FIP MC90 formulation. The CEB-FIP MC90 formulation also [5] determines the shrinkage component.

In this model, the constitutive relationship between stress and strain is

$$\dot{\boldsymbol{\sigma}} = \boldsymbol{D} : \dot{\boldsymbol{\varepsilon}}^{e} = \boldsymbol{D} : \dot{\boldsymbol{\varepsilon}} - \boldsymbol{D} : \dot{\boldsymbol{\varepsilon}}^{sh} - \boldsymbol{D}^{*} : \dot{\boldsymbol{\varepsilon}}^{cr} \tag{7}$$

where $\dot{\boldsymbol{\varepsilon}}^{sh}$ and $\dot{\boldsymbol{\varepsilon}}^{cr}$ are the shrinkage and creep strain rate, respectively, while $\boldsymbol{D}$ and $\boldsymbol{D}^{*}$ denote the fourth-order isotropic elastic linear constitutive tensor and modified constitutive tensor that incorporates the aging of the concrete, respectively. Due to the time integration scheme for the Newton-Raphson algorithm, the Eq. (7) is given by:

$$\boldsymbol{\sigma}_{n+1} = \boldsymbol{\sigma}_{n} + \boldsymbol{D} : \Delta\boldsymbol{\varepsilon} - \boldsymbol{D} : \Delta\boldsymbol{\varepsilon}^{sh} - \boldsymbol{D}^{*} : \Delta\boldsymbol{\varepsilon}^{cr} \tag{8}$$

in which the increment of shrinkage strain is:

$$\Delta\boldsymbol{\varepsilon}^{sh} = \Delta\varepsilon_{sh}(t_s)\mathbf{1} \tag{9}$$

where t_s represents the concrete curing time, and $\Delta\varepsilon_{sh}$ is the variation of magnitude of the concrete deformation by shrinkage, determined using the expressions of CEB-FIP MC90 [5]. To calculate the increment of creep strain, denoted as $\Delta\boldsymbol{\varepsilon}^{cr}$, we use the incremental algorithm developed by Bažant and Prasannan [2; 3], with an adjustment to incorporate CEB-FIP MC90 formulation. This adaptation is possible comparing the creep functions $\boldsymbol{J}(t, t_0)$ of both references. This gives to the following equivalence:

$$E_0 = E_c(t_0),\ \gamma_c(t - t_0) = \beta_c(t - t_0),\ \frac{1}{\upsilon(t)} = \frac{\phi_0}{E_{ci}} \text{ and } \frac{1}{\eta(t)} = 0 \tag{10}$$

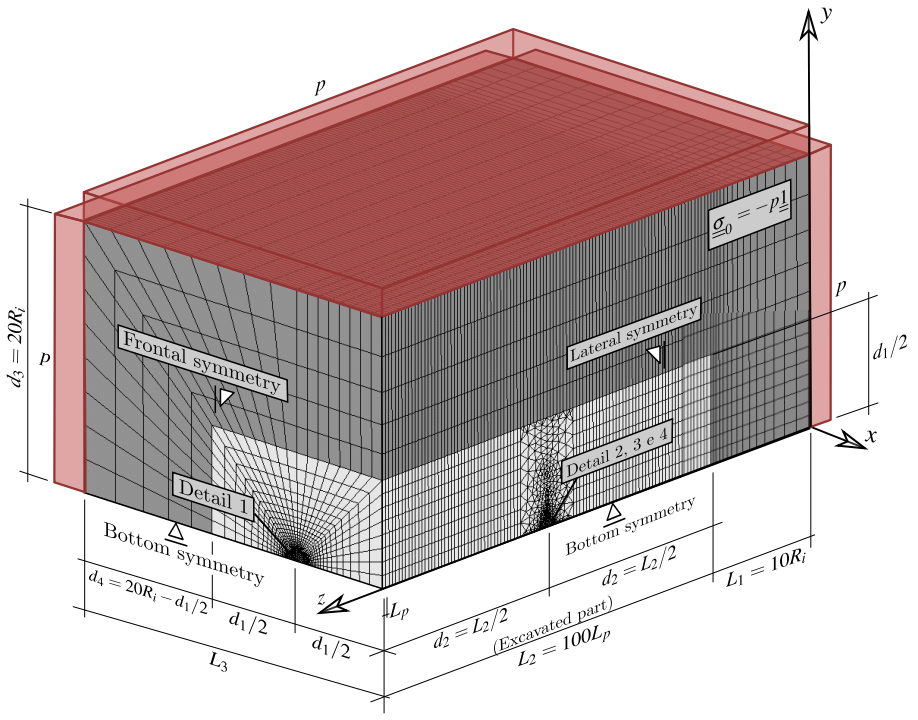

Figure 3: Mesh, dimensions and boundary conditions of the 3D twin tunnel domain

in which, according to Bažant and Prasannan [2; 3], E_0 is the modulus of elasticity of the concrete aggregates and microscopic particles of the cement paste, $\gamma_c(t - t_0)$ is the microviscoelastic deformation of the volume fraction of solidified concrete $v(t)$, $\eta(t)$ is the apparent macroscopic viscosity and, according to CEB-FIP MC90 [5], $E_c(t_0)$ is the tangent elastic modulus of the concrete at the instant of loading application t_0, $\beta_c(t - t_0)$ is a coefficient that depends on the loading age $t - t_0$, ϕ_0 is a coefficient that depends on the age of the concrete at the instant of loading application and E_{ci} the tangent elasticity modulus of the concrete at the age of 28 day.

Details of this model, including validations and its application in single tunnel, are in [8]. See [6] for the algorithm details implemented in FORTRAN within the USERMAT subroutine.

5. Numerical model

The spatial discretization of the domain corresponds to a mesh with trilinear hexahedral elements (SOLID 185), except in the gallery region, which uses higher-order tetrahedral elements (SOLID186). Fig. 8 shows the mesh, geometric parameters, and boundary conditions for the domain problem. In this figure, d_1 is the distance between longitudinal tunnel axes, R_i longitudinal tunnel cross-section radius, L_2 total excavated length, d_3 domain height, L_1 length of the unexcavated region, L_3, L_p step length of the excavation process, d_2 position of the gallery along the longitudinal tunnel. We considered front, side, and bottom symmetry to reduce computational cost. In conjunction with boundary pressure p, we apply the initial stress condition σ_0 at all integration points to simulate the initial state of an undisturbed rock mass, i.e., a zero deformation field before excavation begins. We checked the vertical distortion of the elements away from the tunnel influence zone to reduce the number of elements in this area. Due to the low deformation gradient in this region away from the tunnel wall, the elements in this area can be significantly larger than in others.

Fig. 4 shows the mesh at the cross-section of the longitudinal tunnel, with e representing the thickness of the lining. This article investigates the impact of the spacing d_1 between twin tunnels. Fig. 5 and Fig. 6 illustrate the spatial discretization at the region of the gallery with the longitudinal tunnel, with the spacing $d_1 = 16R_i, 8R_i$ and $4R_i$.

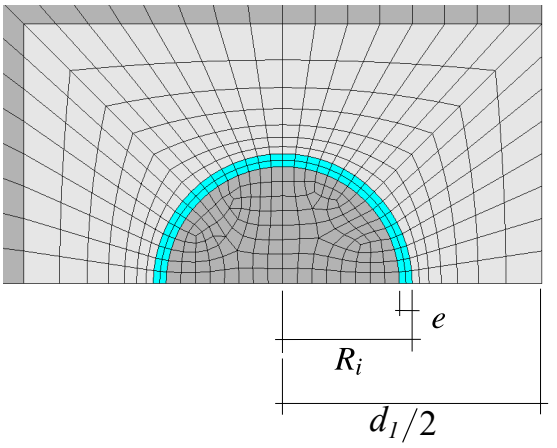

Figure 4: Detail 1 - Mesh in Longitudinal Tunnel cross-section with spacing $d_1 = 4R_i$

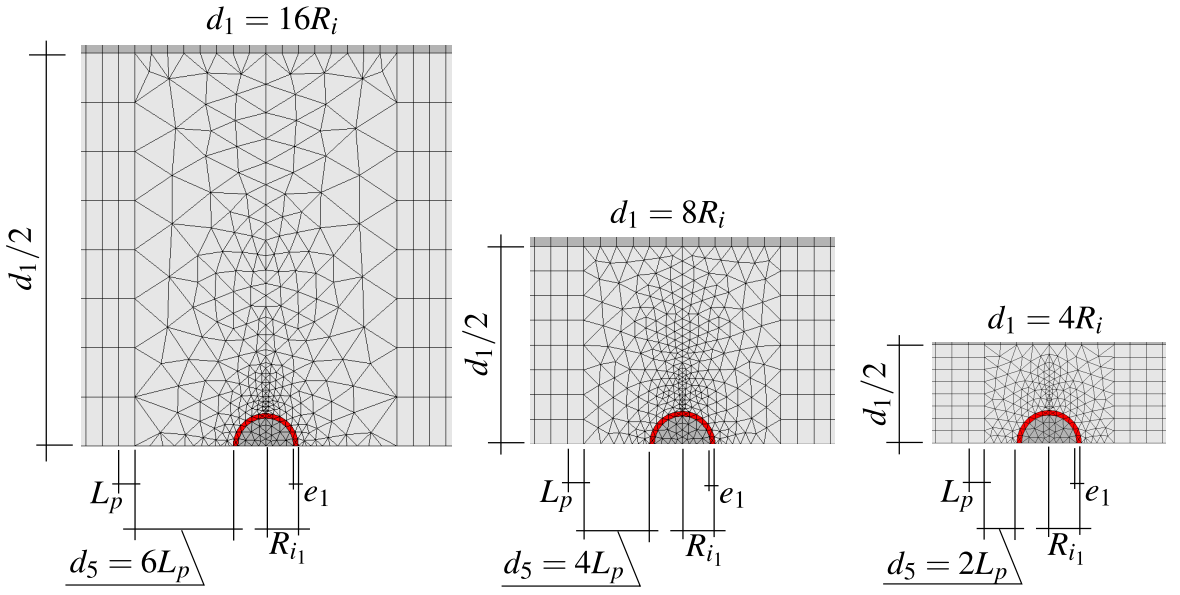

Figure 5: Detail 2 - Side view of the mesh in gallery region with $d_1 = 16R_i$, $d_1 = 8R_i$ and $d_1 = 4R_i$

The construction process involves the activation and deactivation of elements, with a substantial reduction in the stiffness of the excavated element and the adoption of the constitutive law for lining elements. Consequently, during excavation, the rock mass elements under the tunnel are deactivated, while the lining elements activate at a distance d_0 from the excavation face (unlined length). In each excavation step, we execute the solution, and time advances based on the expression $t_p = L_p/V_p$, where L_p represents the length of the excavation step, and V_p is the speed of the excavation face. Figure 4 shows a schematic of the excavation process where n_p is the number of steps excavation.

6. Comparision with analytical solutions

7. Numerical Results and Discussion

Resultados devem ser claros e concisos

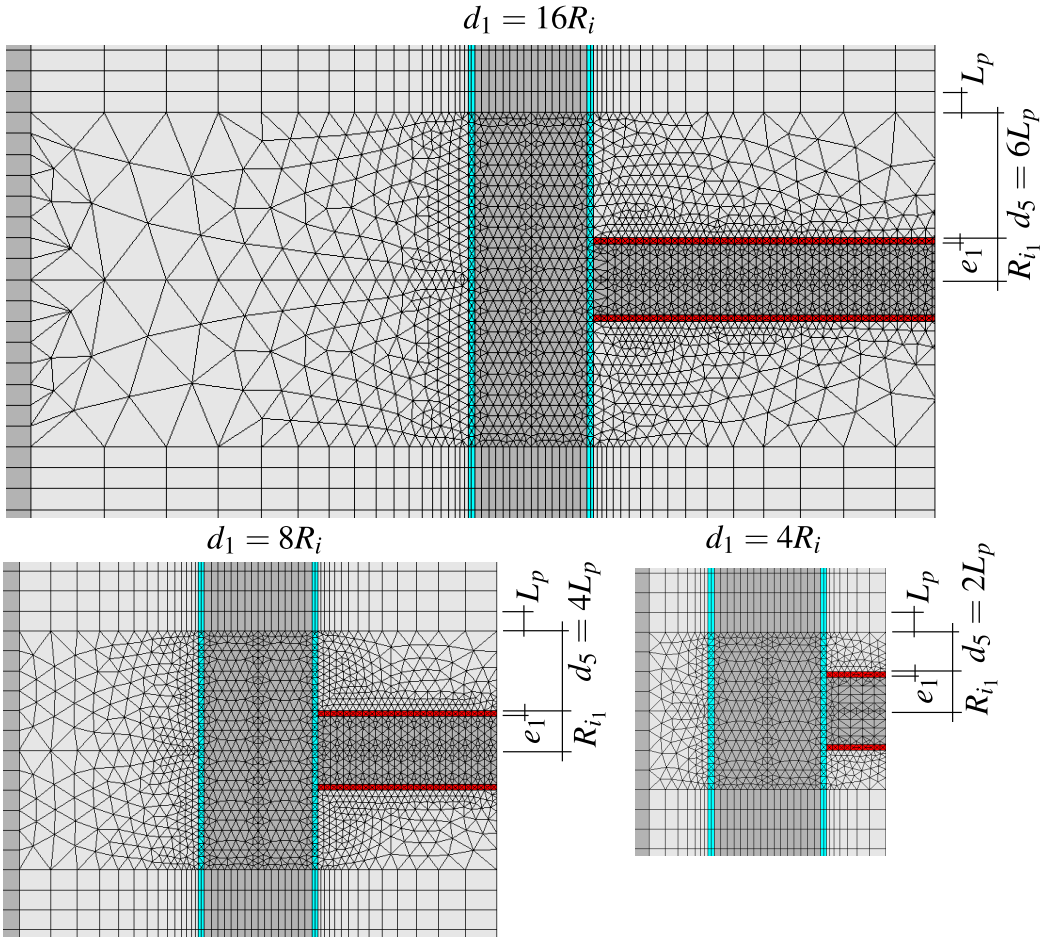

Figure 6: Detail 3 - Bottom view of the mesh in gallery region with $d_1 = 16R_i$, $d_1 = 8R_i$ and $d_1 = 4R_i$

7.1. Influência do afastamento entre os túneis
7.2. A influência da rigidez do revestimento
7.3. A influência da presença da galeria no túnel longitudinal
7.4. Abrangencia da região de influência da galeria
7.5. A influência dos modelos que envolve efeitos diferidos

8. Conclusions

As principais conclusões do estudo podem ser apresentadas numa breve secção de Conclusões, que pode ser autónoma ou constituir uma subsecção de uma secção de Discussão ou de Resultados e Discussão.

9. Appendices

Se houver mais do que um apêndice, estes devem ser identificados como A, B, etc. As fórmulas e equações dos apêndices devem ser numeradas separadamente: Eq. (A.1), Eq. (A.2), etc.; num apêndice seguinte, Eq. (B.1) e assim por diante. O mesmo se aplica aos quadros e figuras: Tabe a A.1; Fig. A.1, etc.

References

ANSYS, 2013. ANSYS Programmer's Reference; release 15.0. Canonsburg, Pennsylvania.
Bažant, Z.P., Prasannan, S., 1989a. Solidification theory for concrete creep. i: Formulation. Journal of engineering mechanics 115, 1691–1703.

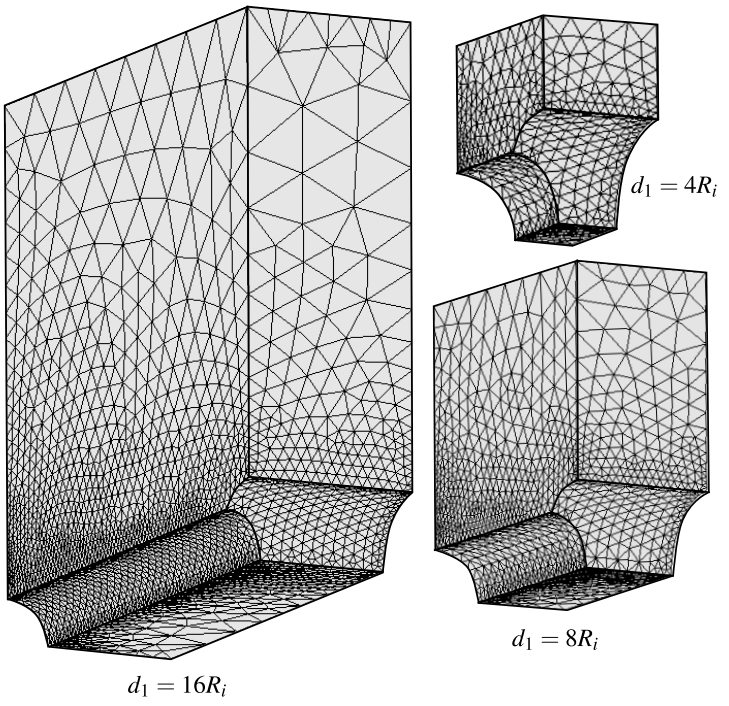

Figure 7: Detail 4 - Isometric view of the portion of the mesh in gallery region $d_1 = 16R_i$, $d_1 = 8R_i$ and $d_1 = 4R_i$

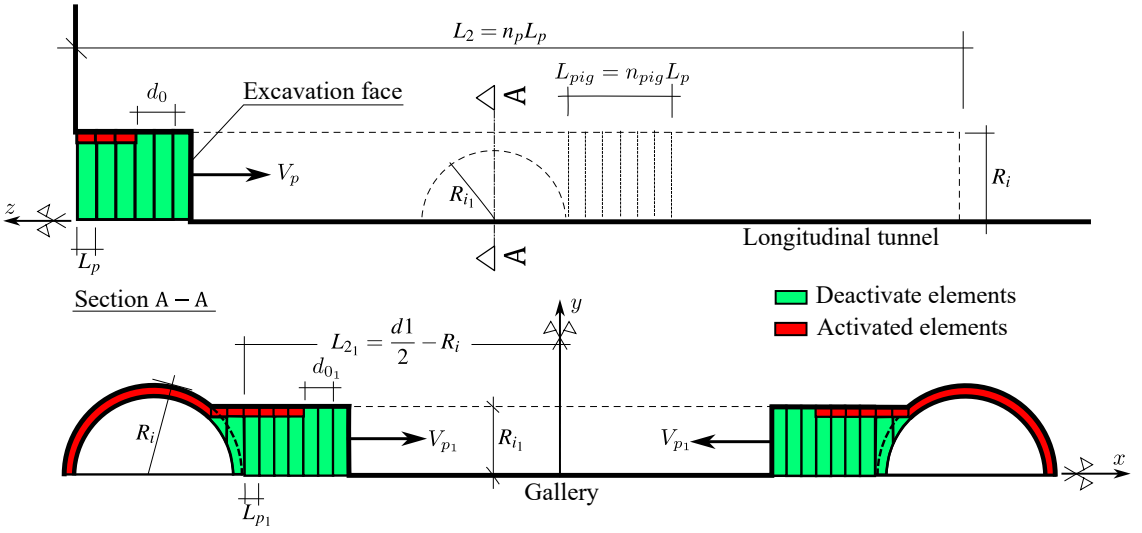

Figure 8: Schematic of the excavation process

Bažant, Z.P., Prasannan, S., 1989b. Solidification theory for concrete creep. ii: Verification and application. Journal of engineering mechanics 115, 1704–1725.

Bernaud, D., 1991. Tunnels profonds dans les milieux viscoplastiques: approches expérimentale et numérique. Ph.D. thesis. Ecole Nationale des Ponts et Chaussées. Paris, French.

CEB-FIP, 1993. CEB-FIP model code 1990: Design code. Comité Euro International du Béton and Fédération Internationale de la Précontrainte (CEB-FIP).

Quevedo, F.P.M., 2017. Comportamento a longo prazo de túneis profundos revestidos com concreto: modelo em elementos finitos. M.S. thesis. Federal University of Rio Grande do Sul. Porto Alegre, Brazil.

Quevedo, F.P.M., 2021. Análise computacional das deformações em túneis profundos considerando o acoplamento plasticidade-viscoplasticidade.

Quevedo, F.P.M., Bernaud, D., Campos Filho, A., 2022a. Numerical analysis of deep tunnels in viscoplastic rock mass considering the creep and shrinkage of the concrete lining. International Journal of Geomechanics 22. doi:10.1061/(ASCE)GM.1943-5622.0002282.

Quevedo, F.P.M., Bernaud, D., S., M., 2022b. Numerical integration scheme for coupled elastoplastic–viscoplastic constitutive law for tunnels. International Journal of Geomechanics 22. doi:10.1061/(ASCE)GM.1943-5622.0002512.